Scheduled Controller Design for Systems With Varying Sensor Configurations: A Frequency-Domain Approach

Robert van der Weijst, Bas van Loon, Marcel Heertjes, and Maurice Heemels, *Fellow, IEEE*

***Abstract*— A novel parameter-dependent scheduled controller design is proposed for systems which exhibit switched dynamics. Switching is a result of varying sensor configurations available in the measurement system. The control architecture is based on *a priori* designed local linear time-invariant controllers, which are designed using frequency-domain loop-shaping techniques. Moreover, conditions on measured frequency response function data of the plant are provided under which the closed-loop system is input-to-state stable for arbitrarily fast parameter variations based on a generalized version of the circle criterion. By presenting a design and analysis framework for scheduled control systems that is easily implementable in existing control software, and does not require parametric plant models, this paper connects well to the industrial control practice. The effectiveness of the proposed scheduling technique, as a way to improve both transient and steady-state performance, is demonstrated by means of a case study which includes measurement results obtained from an industrial wafer stage system.**

***Index Terms*— Circle criterion, frequency-domain, input-to-state stability (ISS), loop-shaping, switched systems, wafer scanners.**

I. Introduction

HIGH-PRECISION motion stages, such as positioning devices used in the semiconductor industry, are subject to ever increasing requirements on stage acceleration (throughput) and positioning accuracy (imaging quality), see [1]. As a result, the influence of structural mode deformation in these stages cannot be neglected. The sensor configuration, i.e., the amount and location of the sensors used in the measurement system, yields a specific characterization of these structural dynamics and is therefore essential for control. In many practical situations, the availability of sensors depends on the position of the motion stage as individual sensors can fall "out-of-range" as a result of physical limitations on their operating ranges. As a result, the sensor configuration may vary as a function of the stage position, which essentially makes the stage, from a control point-of-view, a switched system, see [2], or a position-dependent dynamical system. This complicates the overall design significantly, certainly if the design techniques have to connect to the state-of-the-art industrial control context, which favors data-based frequency-domain conditions in many cases, see [3]. In fact, an important open problem is the design of control systems for dynamical systems with switching sensor configurations based on frequency-domain tools, such as loop-shaping techniques, see [4], [5]. The major advantage of these tools is that they do not necessarily require parametric plant models but can be based on easy-to-obtain (and accurate) measured frequency response functions (FRFs) characterizing the system dynamics, see [3]. Hence, they allow the control engineer to design linear time-invariant (LTI) controllers for both stability and performance using the (measured) FRF of the open-loop transfer function (by means of a Nyquist diagram) or via closed-loop FRFs, such as the sensitivity function and the complementary sensitivity function, see [5]. In the context of switched systems, such a design approach forms a tremendous challenge and many existing approaches do not meet the desired design requirements.

In industry, the problem of position-dependent dynamics is often dealt with by means of robust control design, see [6], in which the authors proposed an $\mathcal{H}_\infty$-controller for this purpose. Although such an approach connects well to techniques of which control engineers are accustomed to, it often results in conservatism, because one single LTI controller is active within the whole range of operation. To overcome this conservatism, several (nonlinear) control techniques exist in the literature that can adapt the controller dynamics according to the online measured actual position of the system. One of these techniques is gain scheduling, see [7], [8]. In gain scheduling, the designer typically selects a finite grid of operating points within the whole range of operation. For each of these operating points FRFs are identified, and based on these FRFs, dedicated local LTI controllers are designed which are connected in the implementation by interpolation. Although the design and implementation is intuitive for control engineers, no constructive results exist to formally and systematically guarantee stability and performance of the closed-loop gain-scheduled system. Another technique is linear parameter-varying (LPV) control, see [9]–[11], which

Manuscript received February 12, 2016; revised November 1, 2016; accepted January 30, 2017. Date of publication March 17, 2017; date of current version February 8, 2018. Manuscript received in final form February 20, 2017. This work was supported by the Dutch Technology Foundation (STW) through the Project HyperMotion: Hybrid Control for Performance Improvement of Linear Motion Systems under Project 10953. Recommended by Associate Editor R. N. Shorten.

R. van der Weijst, B. van Loon, and M. Heemels are with the Control Systems Technology Group, Department of Mechanical Engineering, Eindhoven University of Technology, 5600MB Eindhoven, The Netherlands (e-mail: r.v.d.weijst@tue.nl; s.j.l.m.v.loon@tue.nl; m.heemels@tue.nl).

M. Heertjes is with the Control Systems Technology Group, Department of Mechanical Engineering, Eindhoven University of Technology, 5600MB Eindhoven, The Netherlands, and also with ASML the Netherlands B. V., 5504DR Veldhoven, The Netherlands (e-mail: m.f.heertjes@tue.nl).

Color versions of one or more of the figures in this paper are available online at http://ieeexplore.ieee.org.

Digital Object Identifier 10.1109/TCST.2017.2675838

leads to parameter-dependent controllers. This technique typically requires a parametric model that describes how the dynamics of a system vary as a function of the position. Compared with our approach, obtaining such parametric models is time-consuming and often they are still not accurate enough to properly describe the system dynamics. However, opposed to gain scheduling, the synthesis of LPV controllers yields *a priori* guaranteed stability and performance properties of the LPV controlled system. Nevertheless, LPV control typically requires solving linear matrix inequalities (LMIs), which from an industrial point-of-view is not easy to adopt as it does not connect to the state-of-the-art industrial design tools. In [12], a controller interpolation technique is proposed for LTI systems with multiple objectives. Although this technique seems closely related to the aforementioned gain scheduling techniques, the conditions in [12] do yield a robustly stable control design, based on a finite set of local controllers that is stabilizing for the considered LTI system. Compared with our data-based design and analysis conditions, in [12], parametric models are required, whereas bilinear matrix inequalities need to be solved which not only result in a suboptimal control solution, it also does not meet the standards in industry. Also many designs for the control of switched systems, see [2], [13], [14] require accurate parametric models and LMI-based designs that are not so easily embraced by control engineers in industry. Consequently, there is often a need for design tools for switched systems, such as the class of dynamical systems with position-dependent switching of sensor configurations studied in this paper, that bridge the gap between hybrid systems theory (with formal stability guarantees) and industrial control practice, commonly exploiting frequency-domain design tools and nonparametric models, such as measured FRF descriptions of the motion system dynamics.

In this paper, we provide a solution for such an exemplary design problem in the context of industrial motion stages used in the lithography industry. In particular, we introduce a relevant industrial control problem in this context. Accordingly, we present a design study of a novel scheduled controller that, based on the exogenous reference (x, y)-position of the system, switches between dedicated (local) LTI controllers to control the vertical z-position. The controller has a specific architecture that by design aids the stability analysis and which compares with other architectures [15]. The proposed scheduled controller is intuitive for control engineers because of the following specific design choices: 1) all the individual LTI controllers can be designed using classical frequency-domain loop-shaping techniques based on measured FRFs; 2) graphical data-based conditions can be employed to verify the stability of the closed-loop system under arbitrary switching; and 3) the control architecture allows for the implementation of all components in a standard motion control software environment. The practical feasibility of the proposed approach is emphasized by means of a case study on an industrial motion wafer stage, which is also used to demonstrate the potential of the proposed scheduled controller by measurement results, including the improvements it provides with respect to the state-of-the-art industrial control solution.

This paper significantly extends the preliminary results presented in [16], in particular by presenting: 1) a more detailed modeling section; 2) all the mathematical proofs; and 3) an extensive validation of our proposed results on an industrial wafer stage system, the latter being the key motion system of a wafer scanner that is used in the production of integrated circuits (ICs).

The remainder of this paper is organized as follows. In Section II, we will provide the problem formulation and introduce the plant model in the form of a switched system. In Section III, the proposed control design is introduced and in Section IV, conditions for stability are provided. Finally, experimental results are given in Section V and we will end with the conclusions in Section VI.

II. System and Problem Description

This section considers the modeling of systems with varying sensor configurations. A general mathematical model in the form of a dynamical model with switched output matrices is introduced in Section II-A. In Section II-B, we formulate the problem considered in this paper. A case study of an industrial wafer stage system is introduced in Section II-C, in which we also demonstrate that this system belongs to the model class as introduced in Section II-A.

A. Switched System Formulation

The considered class of systems is given by the following switched single-input-multiple-output model:

$$\mathcal{P}: \begin{cases} \dot{x}_{\mathcal{P}}(t) = A_{\mathcal{P}} x_{\mathcal{P}}(t) + B_{\mathcal{P}} u_{\mathcal{P}}(t) & \text{(1a)} \\ y_{\mathcal{P}_0}(t) = C_{\mathcal{P}_0} x_{\mathcal{P}}(t) & \text{(1b)} \\ y_{\mathcal{P}_1}(t) = \begin{cases} C_{\mathcal{P}_1} x_{\mathcal{P}}(t), & \text{if } \theta(t) \in \Lambda \\ \varnothing, & \text{if } \theta(t) \notin \Lambda \end{cases} & \text{(1c)} \end{cases}$$

with $x_{\mathcal{P}} \in \mathbb{R}^{n_{\mathcal{P}}}$ the state vector, $n_{\mathcal{P}}$ the number of states, $A_{\mathcal{P}} \in \mathbb{R}^{n_{\mathcal{P}} \times n_{\mathcal{P}}}$, $B_{\mathcal{P}} \in \mathbb{R}^{n_{\mathcal{P}} \times 1}$, input $u_{\mathcal{P}} \in \mathbb{R}$, $C_{\mathcal{P}_i} \in \mathbb{R}^{1 \times n_{\mathcal{P}}}$, outputs $y_{\mathcal{P}_i} \in \mathbb{R}$, $i = 0, 1$, where $\varnothing$ indicates that the corresponding output is unavailable, $\theta(t) \in \Theta \subset \mathbb{R}^{n_\theta}$ denotes a vector of n_θ exogenous time-varying parameters, and $\Lambda \subset \Theta$. We associate the following minimal order single-input-single-output (SISO) transfer functions:

$$\mathcal{P}_i(s) = \frac{y_{\mathcal{P}_i}(s)}{u_{\mathcal{P}}(s)}, \quad i = 0, 1, \tag{2}$$

to the corresponding plant outputs, with $s \in \mathbb{C}$ and $u_{\mathcal{P}}(s)$, $y_{\mathcal{P}_0}(s)$, and $y_{\mathcal{P}_1}(s)$ the Laplace variables of the corresponding time-domain signals. Throughout this paper, all Laplace variables and transfer functions are recognized by the (s) argument. Furthermore, the following expression is introduced to describe (2):

$$\mathcal{P}_i(s) = \mathcal{F}(s) \Delta_{\mathcal{P}_i}(s), \quad i = 0, 1, \tag{3}$$

in which all common (shared) dynamics (which are typically present) are contained in $\mathcal{F}(s)$ and specific (nonshared) dynamics are captured in $\Delta_{\mathcal{P}_i}(s)$, $i = 0, 1$, in such a way that no pole-zero cancelations occur in (3).

B. Existing Solution and Problem Description

To motivate the problem addressed in this paper, let us first consider a typical control solution currently used in industry. In this approach, one single SISO LTI controller $\mathcal{C}(s)$ is designed (using frequency-domain loop-shaping techniques), based on FRFs of $\mathcal{P}_0(s)$ and $\mathcal{P}_1(s)$, such that an asymptotically stable closed-loop system results for both *individual* plants. Subsequently, in order to apply $\mathcal{C}(s)$, an output scheduling law is introduced for (1) resulting in the LPV system

$$\dot{x}_{\mathcal{P}}(t) = A_{\mathcal{P}}x_{\mathcal{P}}(t) + B_{\mathcal{P}}u_{\mathcal{P}}(t) \tag{4a}$$

$$y_{\mathcal{P}}(t) = (1-\phi(\theta))C_{\mathcal{P}_0}x_{\mathcal{P}}(t) + \phi(\theta)C_{\mathcal{P}_1}x_{\mathcal{P}}(t) \tag{4b}$$

with $y_{\mathcal{P}}(t) \in \mathbb{R}$, and $\phi : \theta \to [0,1]$ a position-dependent scheduling function for which it holds that $\phi(\theta) = 0$ when $\theta(t) \notin \Lambda$. This method has two significant drawbacks.

1) There is no (*a priori*) guarantee for the stability of the closed-loop connection of (4) with $\mathcal{C}(s)$ for $\theta(t) \in \Theta$ varying over time.
2) Control of both $\mathcal{P}_0(s)$ and $\mathcal{P}_1(s)$ with the same controller $\mathcal{C}(s)$ potentially limits performance.

Note that problem 1) can be solved by selecting $\phi(\theta) = 0$ for all $\theta(t) \in \Theta$, however, in terms of performance, it is beneficial to use $\mathcal{P}_1(s)$ when possible, because typically its output $y_{\mathcal{P}_1}$ gives better measurement information of the relevant dynamics. This is explained in more detail in Section II-C, for the considered case study in that section.

Therefore, in this paper, we consider the problem of a scheduled control design that solves both drawbacks by providing data-based stability conditions that guarantee stability under arbitrary fast variations of $\theta(t)$, while the desired property that the individual controller design for $\mathcal{P}_0(s)$ and $\mathcal{P}_1(s)$ (using loop-shaping techniques) is maintained, thereby connecting to the industrial controller design practice.

C. Case Study: Industrial Wafer Stage

In the remainder of this section, a case study of a wafer stage system is introduced which illustrates the considered problem. In Section V, the proposed scheduled control architecture is experimentally validated on this wafer stage system.

The wafer stage, schematically shown in Fig. 1, is a module of a wafer scanner, which is a device used to expose silicon wafers to a light source from an optical column as part of the production process of ICs, see [1], [17]. The positioning-module (PM) supports a wafer and positions it with respect to the stationary light source along the axes indicated in Fig. 1. More precisely, the PM performs a scanning motion, as the wafer is subject to a meander-like exposure pattern covering the complete wafer surface. The light path (not depicted) enters the stage in negative z-direction at a fixed (x, y)-position (typically the center of the depicted stage). In this respect, the so-called point-of-interest (POI) is defined as the intersection of the light path and the surface of the wafer. As the light path is stationary while the PM is in scanning motion, the POI is time-varying with respect to the PM. In order to meet high-precision overlay (ability to place two layers on top of each other) and focus specifications, accurate position control of the POI in the (x, y)-plane and the z-direction, respectively,

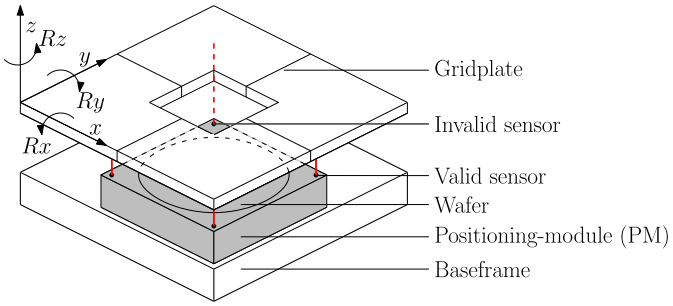

Fig. 1. Schematic representation of a wafer stage.

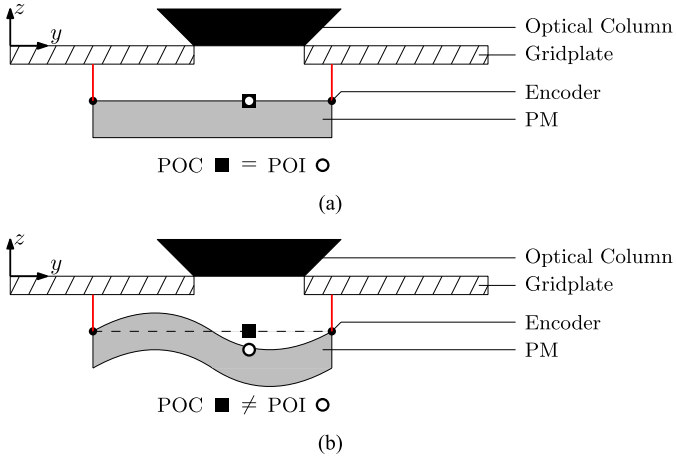

Fig. 2. Schematic representation of a wafer stage in 2-D, illustrating the difference between POC and POI with a structural mode deformed PM. (a) No structural mode deformation. (b) With structural mode deformation.

is crucial. Moreover, positioning should be fast enough, to meet throughput requirements.

As a result of structural mode deformation of the PM, which at the nanometer level is inevitable in practice, POI-control is not straightforward. This problem is shown in Fig. 2, where it can be seen that in general, the POI is not equal to the position estimated by the measurement system, the so-called point-of-control (POC) [Fig. 2(b)], which in general is based on the rigid body position estimate. The common way to improve upon this is to decouple structural mode deformation from the measured PM position and control these modes separately, such that the PM as a whole behaves more like a rigid body, Fig. 2(a). This, however, requires: 1) A structural model of the PM and 2) the number of actuators and sensors to be larger than six, because in any case, the six rigid body modes (x, y, Rz, z, Rx, Ry) have to be controlled. The six *rigid* body modes are independent dynamical modes as a result of the decoupled design of the wafer stage. Therefore, it is common practice in industry to limit feedback control to control the rigid body modes only, see [1], [6]. In this context, it is important that the position measurement system provides a good rigid body position estimate. The considered wafer stage has six actuators, and either six, or eight position measurements, as will become clear in the remainder of this section. As a result, we can only control the PM rigid body modes.

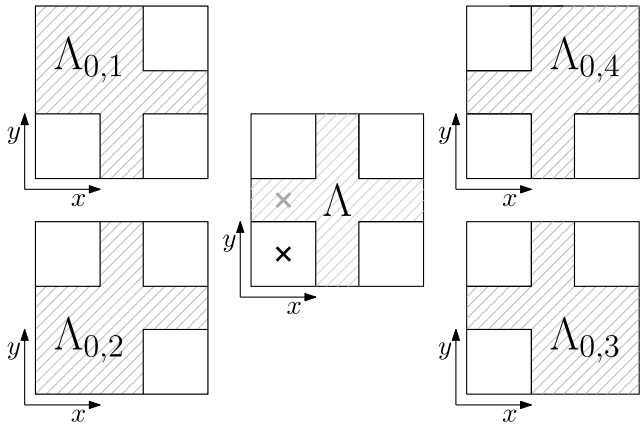

Fig. 3. Partitions of the (x, y) operating range Θ. Note that $\Lambda_1 = \bigcap_{i=1}^{4} \Lambda_{0,i}$. The crosses indicate the positions at which FRF measurements are done, resulting in the two plant descriptions as shown in Fig. 4.

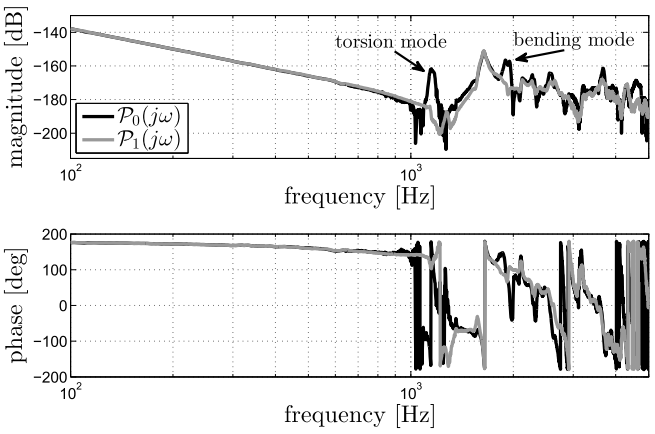

Fig. 4. Measured FRFs of the wafer stage z-axis for two different sensor sets from force F_z in [N] to position z in [m].

Consider again Fig. 1. The position measurement system consists of four sensors, indicated by the black dots, and four gridplates. Each sensor provides a 2-D position measurement: A horizontal and a vertical displacement. However, in order to operate, the sensor has to be underneath its corresponding gridplate. Consequently, due to the square hole between the gridplates, which enables exposure of the wafer, each sensor can enter an out-of-range state, depending on the position of the PM in the (x, y)-plane. As such, the PM position measurement is based on either all four sensors, or a (different) set of three sensors, resulting in either eight or six measurement signals. Based on the available sensor information, the PM rigid body position along the axes in Fig. 1, and thereby the POC, is obtained using coordinate transformations. We want to stress that the outcome is merely an *estimate* of the exact rigid body position, because the obtained sensor signals are corrupted with structural mode deformation. As a result of the physical location of the sensors on the PM, see Fig. 1, each sensor configuration yields a specific characterization of these structural mode deformations, and hence results in a specific rigid body position estimate and consequently a specific POC. This effect is particularly clear when all four sensors are available opposed to a set of three. In that case, we have eight measurements to estimate the PM position in six directions, a situation which is referred to as oversensing. Oversensing (in this case) enables decoupling the deformation of two structural modes, thereby improving the rigid body position estimate.

Let the parameter vector $\theta(t)$ be an exogenous signal that denotes the reference position of the center of the PM in the (x, y)-plane operating range $\Theta \in \mathbb{R}^2$. Then, the partition of Θ can be made as schematically shown in Fig. 3, where Λ corresponds to the set of four sensors being available, and $\Lambda_{0,i}$, $i = 1, 2, 3, 4$, to a different set of three sensors being available. This partition is a direct consequence of the geometry of the wafer stage as shown in Fig. 1. As a result of symmetry of the PM, we can assume the measured dynamics of each set of three sensors to be equal. Therefore, we can relate one output matrix $C_{\mathcal{P}_0}$ to the output $y_{\mathcal{P}_0}$ obtained with a set of three sensors. As a result of oversensing, the set with four sensors will yield a different characterization of the PM dynamics. Therefore, we relate output matrix $C_{\mathcal{P}_1}$ to the output $y_{\mathcal{P}_1}$ obtained with four sensors. Under the assumption that the state dynamics of the PM are well described by the LTI model (1a), we see that each axis of the considered wafer stages belongs to the class of systems (1).

Remark 1: For the case study at hand having essentially two sensor configurations, the design study of a scheduled controller poses a relevant and challenging problem. However, for other applications, a control design solution for systems with a larger number of sensor configurations could be of interest as well. This paper could provide valuable first steps in this direction possibly combined with ideas from multiple input-multiple-output circle criteria. However, this extension is beyond the scope of this paper.

To illustrate the difference in observed dynamics, Bode plots of measured FRFs along the z-axis of $\mathcal{P}_0(s)$ and $\mathcal{P}_1(s)$ as in (2) are given in Fig. 4, where $j\omega = s$, with $\omega \in \mathbb{R}$ the frequency. The measurements are performed at the two positions indicated in (the middle plot of) Fig. 3 with crosses ($\times$). Comparing $\mathcal{P}_0(s)$ and $\mathcal{P}_1(s)$, the effect of a varying sensor configuration is obvious, i.e., the FRFs are different. More specific, we see the effect of oversensing from the fact that two flexible modes (the torsion mode at ± 1150 Hz and a bending mode at ± 1900 Hz) that appear in $\mathcal{P}_1(s)$ are absent in $\mathcal{P}_0(s)$. Also, we see shared dynamics, e.g., the -2 dB/decade slope for low frequencies, corresponding to the rigid body mode. In fact, the two poles at $s = 0$ related to this -2 dB/decade slope are contained in $\mathcal{F}(s)$ in (3) as they appear in both $\mathcal{P}_0(s)$ and $\mathcal{P}_1(s)$. These observations justify the description of each of the systems axes with the class of systems introduced in Section II-A.

Remark 2: For the wafer stage, and motion systems in general, the two poles at $s = 0$ (associated with the rigid body mode) are the only poles outside the open left-half-plane (LHP). Under the nonrestrictive assumption that any considered sensor configuration can measure the rigid body mode, these poles are contained in the common dynamics $\mathcal{F}(s)$ in (3). Therefore, we conclude that the specific (non-shared) dynamics contained by $\Delta_{\mathcal{P}_0}(s)$ and/or $\Delta_{\mathcal{P}_1}(s)$ are stable.

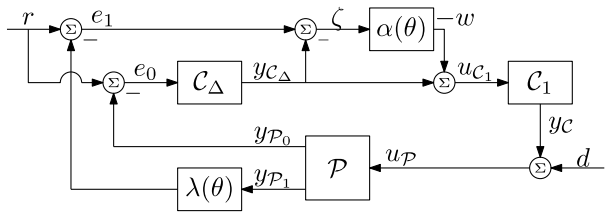

Fig. 5. Proposed scheduled control system schematics.

For the wafer stage system in specific, but motion systems in general, the potential performance increase using scheduled control compared with the state-of-the-art control approach discussed in Section II-B can be explained further. The goal, control of the system's rigid body mode position for reference tracking and disturbance rejection, typically requires high-gain feedback. In this perspective, $\mathcal{P}_1(s)$ is preferable over $\mathcal{P}_0(s)$, for the simple reason that it offers a better rigid body position estimate. Thus, enabling a higher feedback gain without driving the closed-loop system into instability. As already mentioned, $\mathcal{P}_1(s)$ can only be used when $\Theta(t) \in \Lambda$, and hence, switching between $\mathcal{P}_0(s)$ and $\mathcal{P}_1(s)$ and corresponding dedicated controllers can offer better performance than the state-of-the-art solution discussed in Section II-B. This is discussed in more detail in Section V.

III. Scheduled Control Design

In this section, a scheduled control architecture is proposed for the class of systems (1). Note that the wafer stage application discussed in Section II-C fits this setup. First, the specific controller structure, shown in Fig. 5, is motivated, after which the closed-loop system is analyzed.

A. Scheduled Controller Structure

In this section, a novel scheduled controller architecture will be presented, see Fig. 5, that enables control of both $\mathcal{P}_0(s)$ and $\mathcal{P}_1(s)$ with corresponding *a priori* designed dedicated LTI controllers $\mathcal{C}_0(s)$ and $\mathcal{C}_1(s)$. Based on a controller scheduling function $\alpha : \theta \to [0, 1]$, we take the design perspective that either $\mathcal{C}_0(s)$ or $\mathcal{C}_1(s)$ is active, or a "convex combination" of both. Note that for $\mathcal{C}_i(s)$ to be active, the corresponding tracking error $e_i(s) = r(s) - y_{\mathcal{P}_i}(s)$, $i = 0, 1$, should be available, where $r(s)$ denotes the Laplace transform of the reference signal $r(t)$. However, $y_{\mathcal{P}_1}(s)$, and, hence, $e_1(s)$, are only available for $\theta \in \Lambda$. As a result, the scheduling function α should be designed according to the following criterion.

Design Criterion 3: It should hold that the scheduling function α satisfies $\alpha(\theta) = 0$ when $\theta \notin \Lambda$.

Remark 4: Note that for *constant* values of $\alpha \in [0, 1]$, the scalar-valued output $y_{\mathcal{C}}(s)$ of the proposed scheduled controller can be described as

$$y_{\mathcal{C}}(s) = (1 - \alpha)\mathcal{C}_0(s)e_0(s) + \alpha\mathcal{C}_1(s)e_1(s). \tag{5}$$

Although this observation provides intuitive engineering insights, it is important to emphasize that (5) is not a correct representation when α becomes time-varying as in the proposed controller architecture in Fig. 5.

Consider the proposed scheduled control architecture, schematically shown in Fig. 5. Plant $\mathcal{P}$, its input $u_{\mathcal{P}}(t)$, and outputs $y_{\mathcal{P}_i}(t)$, $i = 0, 1$, are as in (1). The input and the output of the $\alpha(\theta)$-block are denoted by scalar variables $\zeta(t)$ and $-w(t)$, respectively, $d(t)$ is an unknown disturbance force. The availability of $y_{\mathcal{P}_1}(t)$ as a function of $\theta(t)$ is modeled by multiplying it by the indicator function $\lambda : \theta \to \{0, 1\}$ given by

$$\lambda(\theta) = \begin{cases} 1, & \text{when } \theta \in \Lambda \\ 0, & \text{when } \theta \notin \Lambda. \end{cases} \tag{6}$$

The proposed control architecture has a specific structure, which is advantageous for achieving a bumpless transfer and for stability analysis. In fact, in Fig. 5, the filter $\mathcal{C}_\Delta(s)$ plays an important role in realizing $\mathcal{C}_0(s)$. Since we aim to design local controllers $\mathcal{C}_0(s)$ and $\mathcal{C}_1(s)$ using frequency-domain loop-shaping techniques, they typically consist of the following filters: A proportional–integral–derivative (PID) filter, a second-order low-pass filter, and a number of notch filters, see [4], [5]. As such, we know that these controllers typically have equal relative degree and they contain some common (shared) dynamics, possibly due to some shared notch filters, but in any case, the pole at $s = 0$ from the PID filter. As a result, to describe $\mathcal{C}_0(s)$ and $\mathcal{C}_1(s)$, we can introduce [similar to (3)] the expressions

$$\mathcal{C}_i(s) = \mathcal{H}(s)\Delta_{\mathcal{C}_i}(s), \quad i = 0, 1, \tag{7}$$

in which all common (shared) dynamics are contained in $\mathcal{H}(s)$ and specific (nonshared) dynamics are captured in $\Delta_{\mathcal{C}_i}(s)$, $i = 0, 1$. Controllers $\mathcal{C}_0(s)$ and $\mathcal{C}_1(s)$ should be designed according to the following criterion, which is not restrictive for the application at hand.

Design Criterion 5: $\mathcal{C}_0(s)$ and $\mathcal{C}_1(s)$ are designed such that no unstable pole-zero cancelations take place in the open-loop connections $\mathcal{P}_i(s)\mathcal{C}_i(s)$, $i = 0, 1$. Furthermore, 1) $\mathcal{C}_1(s)$ is strictly proper[1]; 2) the relative degree of $\mathcal{C}_0(s)$ is larger than or equal to the relative degree of $\mathcal{C}_1(s)$; 3) all poles and zeros of $\mathcal{C}_1(s)$, and all poles of $\mathcal{C}_0(s)$, which lie in the closed right-half-plane, are contained in $\mathcal{H}(s)$; and 4) $\mathcal{H}(s)$, $\Delta_{\mathcal{C}_0}(s)$, and $\Delta_{\mathcal{C}_1}(s)$ are chosen such that no pole-zero cancelations occur in (7).

Note that the two controllers are thus not necessarily constrained to share common elements, i.e., $\mathcal{H}(s)$ might be absent. However, if there are unstable poles or zeros in $\mathcal{C}_1(s)$, $\mathcal{C}_0(s)$ should have the same poles or zeros. Vice versa, if there are unstable poles in $\mathcal{C}_0(s)$, $\mathcal{C}_1(s)$ should have the same poles. This is due to requirement 3) in Design Criterion 5. The structure of the two LTI controllers as in (7) allows us to define the LTI filter $\mathcal{C}_\Delta(s)$ in Fig. 5 as

$$\mathcal{C}_\Delta(s) = \Delta_{\mathcal{C}_0}(s)\Delta_{\mathcal{C}_1}^{-1}(s). \tag{8}$$

In order to derive a state-space realization of the closed-loop dynamics, we introduce the state-space description

$$\mathcal{C}_1 : \begin{cases} \dot{x}_{\mathcal{C}_1}(t) = A_{\mathcal{C}_1}x_{\mathcal{C}_1}(t) + B_{\mathcal{C}_1}u_{\mathcal{C}_1}(t) \\ y_{\mathcal{C}}(t) = C_{\mathcal{C}_1}x_{\mathcal{C}_1}(t) \end{cases} \tag{9}$$

[1]Note that the derivations in the remainder of this paper are valid mutatis mutandis when the controller $\mathcal{C}_1(s)$ is proper. However, since in this application the controllers are naturally strictly proper, we opted to use this strict properness for ease of exposition.

of $\mathcal{C}_1(s)$ with input $u_{\mathcal{C}_1}(t) \in \mathbb{R}$, output $y_{\mathcal{C}}(t) \in \mathbb{R}$, and where we used Design Criterion 5-1). From Design Criterion 5-3), it follows that (8) has all poles in the open LHP [$\mathcal{H}(s)$ contains unstable poles in $\mathcal{C}_0(s)$ and $\mathcal{C}_1(s)$, if present]. From Design Criterion 5-4), it follows that $\mathcal{C}_\Delta(s)$ does not contain any pole-zero cancelations, and finally, from Design Criterion 5-2), it follows that $\mathcal{C}_\Delta(s)$ is proper. Hence, we have that filter $\mathcal{C}_\Delta(s)$ is proper, stable, and the state-space description

$$\mathcal{C}_\Delta : \begin{cases} \dot{x}_{\mathcal{C}_\Delta}(t) = A_{\mathcal{C}_\Delta} x_{\mathcal{C}_\Delta}(t) + B_{\mathcal{C}_\Delta} e_0(t) \\ y_{\mathcal{C}_\Delta}(t) = C_{\mathcal{C}_\Delta} x_{\mathcal{C}_\Delta}(t) + D_{\mathcal{C}_\Delta} e_0(t) \end{cases} \tag{10}$$

can be given with output $y_{\mathcal{C}_\Delta}(t) \in \mathbb{R}$. Note that (9) and (10) are chosen to be minimal realizations, and therefore do not have pole-zero cancelations. Furthermore, the matrix $A_{\mathcal{C}_\Delta}$ is Hurwitz.

Remark 6: The shared controller dynamics $\mathcal{H}(s)$ are in the closed loop irrespective of any of the parameter-varying elements. This is advantageous for bumpless transfer, especially because for the application at hand, the integral action of the PID-type filters, i.e., the pole at $s = 0$, is contained in $\mathcal{H}(s)$. This eliminates scheduling-induced integrator windup, and as such, no integrator conditioning is required, see also [18].

Having discussed the intuition behind the proposed scheduled control architecture, its specific structure, and important (nonrestrictive) design criteria, in the remainder of this section, the closed-loop system is analyzed.

B. Closed-Loop System Analysis

To obtain a state-space description for the closed-loop system, observe that from Design Criterion 3 and (6), it follows that $\lambda(\theta) = 1$ when $\alpha(\theta) \neq 0$, i.e., $\alpha(\theta)\lambda(\theta) = \alpha(\theta)$ for all θ. As a result, we have

$$\begin{aligned} u_{\mathcal{C}_1}(t) &= (1-\alpha(\theta(t)))y_{\mathcal{C}_\Delta}(t) + \alpha(\theta(t))(r(t) - \lambda(\theta(t))y_{\mathcal{P}_1}(t)) \\ &= (1-\alpha(\theta(t)))y_{\mathcal{C}_\Delta}(t) + \alpha(\theta(t))(r(t) - y_{\mathcal{P}_1}(t)). \end{aligned}$$

Hence, $\lambda : \theta \to \{0, 1\}$ does not influence the closed-loop dynamics. Using (1), (9), and (10), we can write the closed loop as the Lur'e-type system [19]

$$\dot{x}(t) = Ax(t) + Bw(t) + B_v v(t) \tag{11a}$$

$$\zeta(t) = Cx(t) + D_v v(t) \tag{11b}$$

$$w(t) = -\alpha(\theta)\zeta(t) \tag{11c}$$

with augmented state vector $x = [x_{\mathcal{P}}^\top \; x_{\mathcal{C}_1}^\top \; x_{\mathcal{C}_\Delta}^\top]^\top$, $v = [r \; d]^\top$, and matrices given by

$$\left[\begin{array}{c|c|c} A & B & B_v \\ \hline C & & D_v \end{array}\right] = \left[\begin{array}{ccc|c|cc} A_{\mathcal{P}} & B_{\mathcal{P}}C_{\mathcal{C}_1} & 0 & 0 & 0 & B_{\mathcal{P}} \\ -B_{\mathcal{C}_1}D_{\mathcal{C}_\Delta}C_{\mathcal{P}_0} & A_{\mathcal{C}_1} & B_{\mathcal{C}_1}C_{\mathcal{C}_\Delta} & -B_{\mathcal{C}_1} & B_{\mathcal{C}_1}D_{\mathcal{C}_\Delta} & 0 \\ -B_{\mathcal{C}_\Delta}C_{\mathcal{P}_0} & 0 & A_{\mathcal{C}_\Delta} & 0 & B_{\mathcal{C}_\Delta} & 0 \\ \hline D_{\mathcal{C}_\Delta}C_{\mathcal{P}_0} - C_{\mathcal{P}_1} & 0 & -C_{\mathcal{C}_\Delta} & & 1-D_{\mathcal{C}_\Delta} & 0 \end{array}\right]. \tag{12}$$

The transfer function from $w(s)$ to $\zeta(s)$ can be obtained from (11) as

$$\mathcal{G}(s) = C(sI - A)^{-1}B$$

with I the identity matrix of appropriate dimensions. The same transfer function can be derived from the system schematics shown in Fig. 5, which gives

$$\mathcal{G}(s) = \frac{\mathcal{P}_0(s)\mathcal{C}_0(s) - \mathcal{P}_1(s)\mathcal{C}_1(s)}{1 + \mathcal{P}_1(s)\mathcal{C}_1(s)}. \tag{13}$$

Remark 7: In case $\mathcal{C}_1(s) \neq \mathcal{H}(s)$, pole-zero cancelations occur in the series connection

$$\mathcal{C}_\Delta(s)\mathcal{C}_1(s) = \Delta_{\mathcal{C}_0}(s)\Delta_{\mathcal{C}_1}^{-1}(s)\Delta_{\mathcal{C}_1}(s)\mathcal{H}(s)$$

which appears in the closed-loop system. Therefore, system (11), (12) is a nonminimal realization by design. Note that due to Design Criterion 5-3) and 4), it follows that this only concerns stable pole-zero cancelations.

In the remainder of this section, we show that the matrix A in (12) is Hurwitz if a set of conditions is satisfied which are summarized in Proposition 8.

Proposition 8: The system matrix A given in (12) is Hurwitz if the following holds.

(i) The transfer function

$$\mathcal{O}_0(s) = \frac{y_{\mathcal{P}_0}(s)}{e_0(s)} = \mathcal{P}_0(s)\mathcal{C}_0(s) \tag{14}$$

satisfies the Nyquist stability criterion [5].

(ii) Design Criterion 5 is fulfilled.

Proof: For a proof see Appendix A. □

Remark 9: Note that the conditions in Proposition 8 are not restrictive. Condition (i) is trivial for a loop-shaped linear controller design and, for the application at hand, Design Criterion 5 is not restrictive by itself.

IV. Stability Analysis

In this section, sufficient data-based conditions for input-to-state stability (ISS) [20] of the closed-loop system (11), (12) are provided.

Definition 10 [20], [21]: The system (11), (12) is said to be ISS if there exist a $\mathcal{KL}$-function β and $\mathcal{K}$-function γ such that for any initial state $x(0) \in \mathbb{R}^{n_x}$ and any (essentially) bounded input signal v, the corresponding solution satisfies

$$|x(t)| \leq \beta(|x(0)|, t) + \gamma(\|v\|_\infty) \tag{15}$$

for all $t \in \mathbb{R}_{\geq 0}$.

To this end, we employ the Lur'e-structure of the closed-loop system, being a feedback interconnection of an LTI system with one scalar parameter-varying gain $\alpha(\theta) \in [0, 1]$. From the circle criterion [19], frequency-domain conditions exist to conclude on absolute stability of the origin of a Lur'e-type system without external inputs, which can be extended to ISS in case the system does have external inputs, see [21], [22]. The main result of this section is given in Theorem 11.

Theorem 11: Consider systems of the form (11), (12), with scheduling function $\alpha : \theta \to [0, 1]$ satisfying Design Criterion 3. Suppose that the following holds.

(I) The system matrix A is Hurwitz.

(II) There exists a constant $\rho > 1$ such that the strictly proper transfer function $\mathcal{G}(s)$, given in (13), satisfies

$$\mathrm{Re}(\mathcal{G}(j\omega)) > -\frac{1}{\rho} \quad \text{for all } \omega \in \mathbb{R}.$$

Then, the system (11), (12), with $\alpha : \theta \to [0, 1]$, is ISS with respect to v and its origin is globally exponentially stable (GES) for $v = 0$.

Proof: For a proof see Appendix B. □

Note that Theorem 11 is based on the circle criterion, which in its typical appearance requires minimality of the underlying LTI system, see [19], [23]. However, as discussed in Remark 7, minimality of system (A, B, C) as in (12) is not necessarily guaranteed. In this respect, we would like to emphasize that, under the additional requirement that the unobservable and/or uncontrollable dynamics are stable, minimality of (A, B, C) as in (12) is not required in Theorem 11. Nevertheless, the circle criterion as provided in [24] seems closely related to our result with the difference that in [24] no explicit statement on minimality is provided, neither a formal proof on whether or not minimality is a necessary requirement for their result. Therefore, it is appropriate to provide a complete proof here, see Appendix B.

V. Wafer Stage Experiments

In this section, the proposed scheduled controller approach is applied to control the z-axis of the motion stage as introduced in Section II-C.

A. Design of the Proposed Scheduled Controller

The scheduled controller is *exactly* implemented as indicated in the block scheme given in Fig. 5, in which the scheduling function $\alpha : \theta \to [0, 1]$ is implemented as a discontinuous switch given by

$$\alpha(\theta) = \begin{cases} 1, & \text{when } \theta \in \Lambda \\ 0, & \text{when } \theta \notin \Lambda \end{cases} \tag{16}$$

which satisfies Design Criterion 3. Note that in (16), $\theta(t)$ is chosen as the exogenous reference position of the PM in the (x, y)-plane, see Section II-C. The LTI controllers $\mathcal{C}_0(s)$ and $\mathcal{C}_1(s)$ are designed using loop-shaping, based on the corresponding plant FRFs $\mathcal{P}_0(s)$ and $\mathcal{P}_1(s)$, see Fig. 4, in such a way that Design Criterion 5 is satisfied. Both controllers consist of a PID filter, a second-order low-pass filter, and a limited number of notch filters, and their Bode diagrams are shown in Fig. 6. As a result, the scheduled controller can be implemented in standard motion control software, because it consists of classical control filters, and the total controller order is only increased with the order of $\mathcal{C}_\Delta(s)$. In this case study, the structure of both controllers is almost identical except for one additional notch filter in $\mathcal{C}_0(s)$, necessary to compensate for the structural mode resonance around ± 1150 Hz in $\mathcal{P}_0(s)$ [which is absent in $\mathcal{P}_1(s)$], see Fig. 4. Without the phase lag introduced by this additional notch filter, $\mathcal{C}_1(s)$ can have a higher gain for frequencies below the bandwidth, thereby increasing the tracking performance, given that the frequency contents of the disturbance $d(t)$ and reference $r(t)$ are typically concentrated at low frequencies. The effect of high-gain feedback on disturbance suppression is clear when we consider the sensitivity functions

$$\mathcal{S}_i(s) = \frac{e_i(s)}{r(s)} = \frac{1}{1 + \mathcal{P}_i(s)\mathcal{C}_i(s)}$$

with $i = 0, 1$, of which Bode plots are shown in Fig. 7.

Stability of each *individual/local* closed loop is verified by means of the Nyquist criterion, see [5] and Fig. 8, which shows robust stability given a modulus margin (MM) of approximately 8 dB. Consequently, the conditions of Proposition

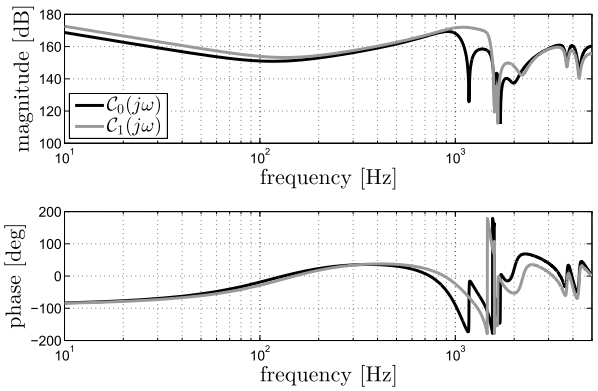

Fig. 6. Bode plots of the controllers $\mathcal{C}_i(j\omega)$, $i = 0, 1$.

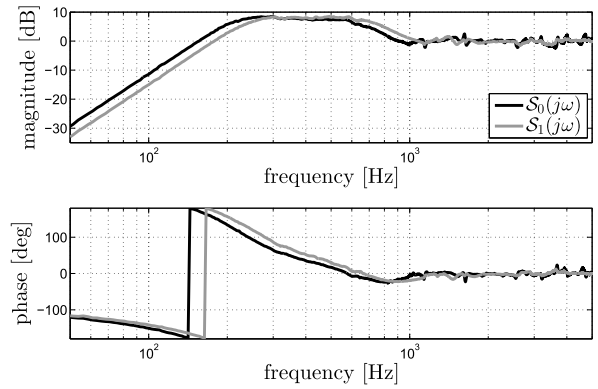

Fig. 7. Bode plots of sensitivities $\mathcal{S}_i(j\omega)$, $i = 0, 1$.

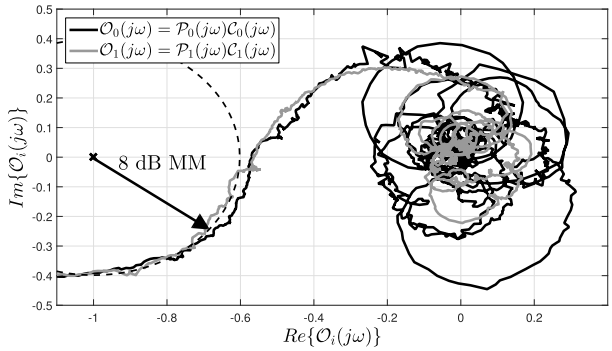

Fig. 8. Nyquist diagrams of $\mathcal{O}_i(j\omega) = \mathcal{P}_i(j\omega)\mathcal{C}_i(j\omega)$, $i = 0, 1$. The dashed circle indicates a modulus margin (MM) of 8 dB.

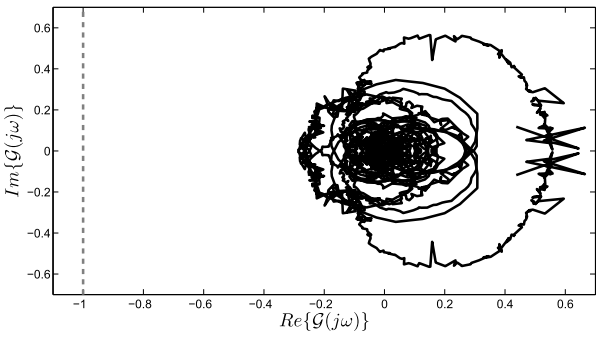

Fig. 9. Polar plot of $\mathcal{G}(j\omega)$ as in (13) in which the dashed line represents -1.

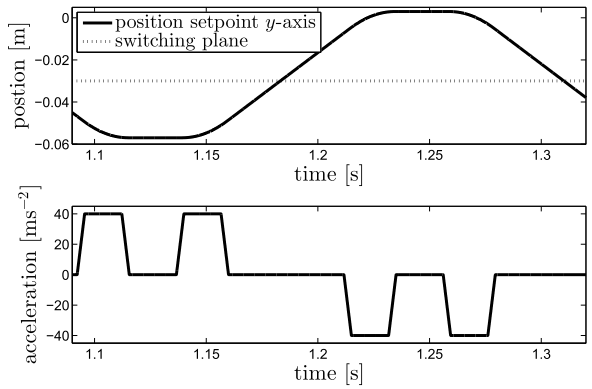

Fig. 10. Position $\theta(t) = r_y(t)$ and acceleration reference signal trajecory along the y-axis and the switching plane at $\theta(t) = \theta^*$.

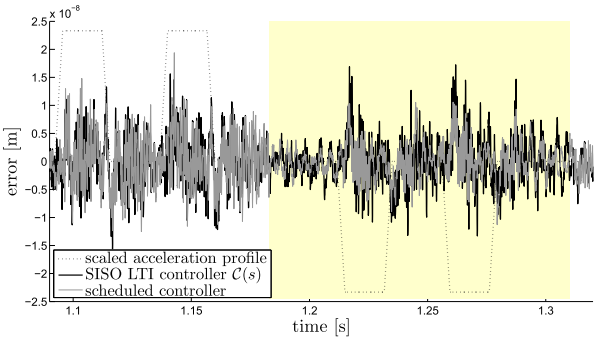

Fig. 11. z-axis error in time-domain. In this figure, $\alpha(\theta) = 1$ in the yellow window and $\alpha(\theta) = 0$ elsewhere.

8 are met, thereby satisfying condition (I) in Theorem 11. The final step in the design is to verify condition (II) in Theorem 11. This condition is verified by means of Fig. 9, which represents the polar plot of $\mathcal{G}(s)$ as in (13), showing that $\rho Re(\mathcal{G}(j\omega)) > -1$, for $\rho > 1$ is met for all $\omega \in \mathbb{R}$ with sufficient margins to account for plant uncertainty. In this respect, note that the user can influence $Re(\mathcal{G}(j\omega))$, and thus condition (II) in Theorem 11, by means of the design of $\mathcal{C}_0(s)$ and $\mathcal{C}_1(s)$. Here, we want to emphasize that the obtained margins in Fig. 9 do not imply that the control design is conservative in terms of performance, as the design for performance is done in the LTI regimes by means of the Nyquist (Fig. 8) and sensitivity (Fig. 7) plots.

B. Experimental Results

In this section, the proposed scheduled controller approach is applied to control the z-axis of the motion stage as introduced in Section II-C. Moreover, we compare the obtained results with those using one single SISO LTI controller $\mathcal{C}(s)$, which is selected as $\mathcal{C}(s) = \mathcal{C}_0(s)$, in combination with $\mathcal{P}_0(s)$, i.e., we apply the state-of-the-art solution as described in Section II-B, with plant description (4) with $\phi(\theta) = 0$ for all θ. Note that the state-of-the-art solution may perform better when we select a varying $\phi(\theta(t))$, this is discussed in Remark 13.

The reference signal used during the experiments is a scanning motion in the y-direction, while all other axes are kept at constant positions. To be more precise, the reference signal in the z-direction is zero, i.e., $r(t) = 0$. As a result, we have that $\theta(t) = r_y(t) \in \mathbb{R}$, with $r_y(t)$ the reference signal in the y-direction, which is shown in Fig. 10. Moreover, for this specific $\theta(t)$, we have that both $\theta \in \Lambda$ and $\theta \notin \Lambda$ occur. As such, combined with the definition of the scheduling function $\alpha : \theta \to [0, 1]$ given in (16), a switching plane results which is characterized by $\theta(t) = \theta^* = -0.03$ [m], and which is also shown in Fig. 10. For $\theta(t) > \theta^*$, we have that $\alpha(\theta) = 1$.

The resulting tracking error in the z-direction in the time-domain is shown in Fig. 11, where the yellow window represents the situation in which $\alpha(\theta) = 1$, whereas $\alpha(\theta) = 0$ elsewhere. From Fig. 11, it is clear that transient effects induced by switching are negligible compared with the disturbance-induced error, at least in terms of absolute value. In the lithographic industry, the accuracy of the wafer stage is often related to overlay and imaging quality, see [1]. Let us first consider overlay, which is the ability of the wafer stage to expose two images exactly on top of each other. In this respect, the moving average (MA) performance measure is of central interest as this forms a measure of the average position error of the wafer stage during exposure, which in turn determines where the image is located on the wafer, hence, a measure for overlay. The MA represents the lower frequency part of the error, and is defined as

$$\text{MA} := \frac{1}{T_e} \int_{-\frac{T_e}{2}}^{\frac{T_e}{2}} e(t)dt$$

in which T_e represents the exposure time, and $e(t)$ represents the position error of the z-axis as a function of time t. The second quality measure is the imaging quality, which is affected by the accuracy of the positioning of the wafer stage, as position errors affect the contrast. In this respect, the moving standard deviation (MSD) performance measure is of central interest, which is defined as

$$\text{MSD} := \sqrt{\frac{1}{T_e} \int_{-\frac{T_e}{2}}^{\frac{T_e}{2}} (e(t) - \text{MA})^2 dt}$$

and represents the higher frequency part of the positioning error. The MA and MSD of the positioning error are shown in Figs. 12 and 13, respectively. In Figs. 12 and 13, the yellow window represents the situation in which $\alpha(\theta) = 1$, whereas

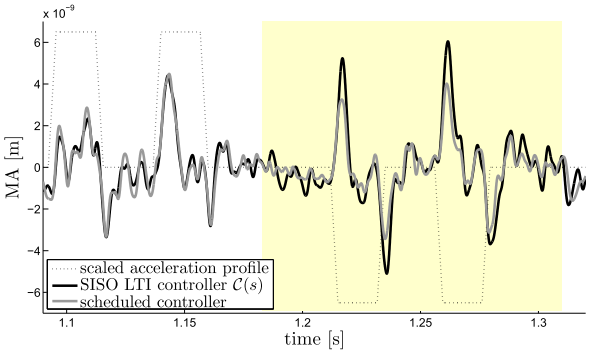

Fig. 12. MA of the z-axis error. In this figure, $\alpha(\theta) = 1$ in the yellow window and $\alpha(\theta) = 0$ elsewhere.

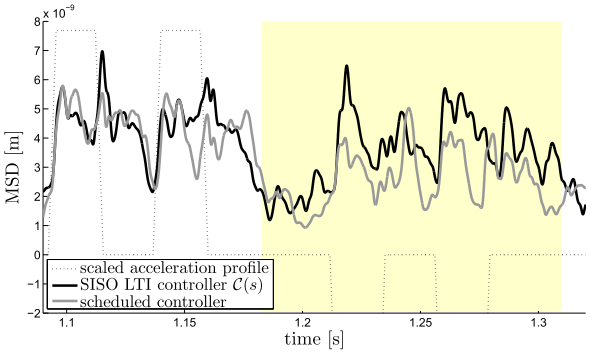

Fig. 13. MSD of the z-axis error. In this figure, $\alpha(\theta) = 1$ in the yellow window and $\alpha(\theta) = 0$ elsewhere.

$\alpha(\theta) = 0$ elsewhere. Clearly, both the MA as well as the MSD values are significantly reduced using our proposed scheduled controller. This can be further clarified by considering Fig. 14, which shows the cumulative power spectral density (CPSD) of the tracking error response of the z-axis for both control strategies. In Fig. 14, we see a performance increase over the complete frequency range which, intuitively, can be explained as follows. For frequencies below the closed-loop bandwidth ($\pm$300 Hz), this is a result of the higher feedback gain of $\mathcal{C}_1(s)$. For frequencies above the bandwidth, this is due to the absence of two structural modes that appear in $\mathcal{P}_0(s)$, at $\pm$1150 and $\pm$1900 Hz, which do not appear in $\mathcal{P}_1(s)$, see Fig. 4.

Remark 12: Note that discontinuous switching might excite high-frequency plant dynamics, and therefore, using smoother scheduling functions $\alpha : \theta \to [0, 1]$ could improve the results even further.

Remark 13: It is mentioned in Section II-B that often, for the state-of-the-art solution, the industrial practice is to select a varying $\phi(\theta(t))$ such that $\mathcal{P}_1$ is used for some $\theta \in \Lambda$, instead of $\mathcal{P}_0$ for all θ. From a performance point-of-view, this might yield a better overall performance as compared with the state-of-the-art solution for frequencies above $\pm$1100 Hz, as for those frequencies, $\mathcal{P}_0(s)$ and $\mathcal{P}_1(s)$ are significantly different, see Fig. 4. Nevertheless, it is also mentioned in Section II-B that such an approach does not automatically yield closed-loop stability. For this reason, we compare the scheduled controller with the state-of-the-art solution with $\phi(\theta) = 0$ for all θ in this section. From this perspective, and for frequencies above $\pm$1100 Hz, the presented results of the state-of-the-art solution, see Fig. 14, might be pessimistic. Nevertheless, for frequencies below $\pm$1100 Hz, the presented performance increase holds, also when compared with the state-of-the-art solution with a varying $\phi(\theta(t))$.

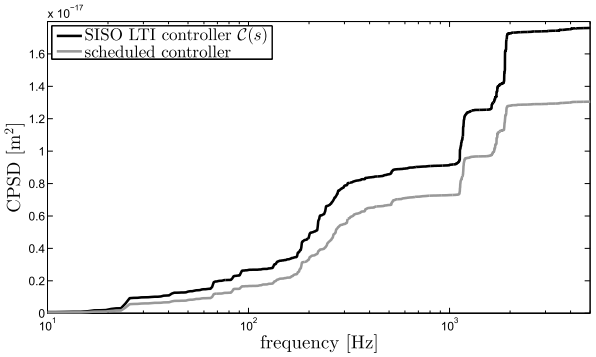

Fig. 14. CPSD of the z-axis error.

VI. Conclusions

In this paper, we proposed a novel scheduled controller architecture for dynamical systems with position-dependent switching sensor configurations in the context of an industrial wafer stage system. Based on the position of the motion system, dedicated (local) LTI controllers are switched ON or OFF. To meet the requirements from industry, we present a design methodology using classical frequency-domain loop-shaping techniques based on measured FRF data, and we choose an architecture that is implementable in a standard software environment. Moreover, easy-to-handle data-based conditions are presented that allow the user to verify whether the scheduled feedback control system is ISS with respect to external disturbances, measurement noise, and reference signals, irrespective of how the switching between the controllers occurs in time. In fact, these frequency-domain conditions are based on a generalized form of the circle criterion for which minimality of the underlying system is not required. The practical feasibility of the proposed controller scheduling architecture, as well as the ability to outperform the state-of-the-art industrial control solution, has been experimentally demonstrated on an industrial wafer stage system.

Appendix A
Proof of Proposition 8

Proof: Without loss of generality, take $\alpha(\theta) = 0$ constant. Then, the scheduled control system is described by (11a), (11b), and the control system schematics, shown in Fig. 5, reduce to a closed-loop interconnection of the filters $\mathcal{P}(s)$, $\mathcal{C}_1(s)$, and $\mathcal{C}_\Delta(s)$, with open-loop transfer function $\mathcal{O}_0(s)$ given by (14). Observe that

$$\mathcal{O}_0(s) = \frac{y_{\mathcal{P}_0}(s)}{e_0(s)} = \mathcal{P}_0(s)\mathcal{C}_0(s) = \mathcal{P}_0(s)\mathcal{C}_\Delta(s)\mathcal{C}_1(s) = \mathcal{P}_0(s)\mathcal{H}(s)\Delta_{\mathcal{C}_1}(s)\Delta_{\mathcal{C}_0}(s)\Delta_{\mathcal{C}_1}^{-1}(s). \quad (17)$$

This observation yields the following state-space model:

$$\mathcal{O}_0 : \begin{cases} \dot{x}(t) = A_{\mathcal{O}_0} x(t) + B_{\mathcal{O}_0} e_0(t) \\ y_{\mathcal{P}_0}(t) = C_{\mathcal{O}_0} x(t) \end{cases} \tag{18}$$

with matrices given by

$$\left[\begin{array}{c|c} A_{\mathcal{O}_0} & B_{\mathcal{O}_0} \\ \hline C_{\mathcal{O}_0} & \end{array}\right] = \left[\begin{array}{ccc|c} A_{\mathcal{P}} & B_{\mathcal{P}} C_{\mathcal{C}_1} & 0 & 0 \\ 0 & A_{\mathcal{C}_1} & B_{\mathcal{C}_1} C_{\mathcal{C}_\Delta} & B_{\mathcal{C}_1} D_{\mathcal{C}_\Delta} \\ 0 & 0 & A_{\mathcal{C}_\Delta} & B_{\mathcal{C}_\Delta} \\ \hline C_{\mathcal{P}_0} & 0 & 0 & \end{array}\right]. \tag{19}$$

System (18) can be a nonminimal realization due to the following two reasons.

1) Pole-zero cancelations can occur in the transfer function (17) as already indicated in Remark 7.
2) The states related to $\Delta_{\mathcal{P}_1}(s)$, defined in (3) (suppose $\Delta_{\mathcal{P}_1}(s)$ is not constant), are not in the minimal realization between $u_{\mathcal{P}}(t)$ and $y_{\mathcal{P}_0}(t)$.

Using a similarity transformation $\bar{x} = T^{-1}x$ for the nonsingular matrix T of appropriate dimensions, we can bring (18), (19) in the Kalman decomposition

$$\begin{aligned} \dot{\bar{x}}(t) &= \bar{A}_{\mathcal{O}_0} \bar{x}(t) + \bar{B}_{\mathcal{O}_0} e_0(t) \\ y_{\mathcal{P}_0}(t) &= \bar{C}_{\mathcal{O}_0} \bar{x}(t) \end{aligned} \tag{20}$$

with

$$\bar{A}_{\mathcal{O}_0} = T^{-1} A_{\mathcal{O}_0} T, \quad \bar{B}_{\mathcal{O}_0} = T^{-1} B_{\mathcal{O}_0}, \ \bar{C}_{\mathcal{O}_0} = C_{\mathcal{O}_0} T \tag{21}$$

and matrices given by

$$\left[\begin{array}{c|c} \bar{A}_{\mathcal{O}_0} & \bar{B}_{\mathcal{O}_0} \\ \hline \bar{C}_{\mathcal{O}_0} & \end{array}\right] = \left[\begin{array}{cccc|c} A_{11} & 0 & 0 & 0 & 0 \\ A_{21} & A_{22} & 0 & 0 & B_2 \\ A_{31} & 0 & A_{33} & 0 & 0 \\ A_{41} & A_{42} & A_{43} & A_{44} & B_4 \\ \hline C_1 & C_2 & 0 & 0 & \end{array}\right]. \tag{22}$$

Because $\bar{A}_{\mathcal{O}_0}$ is lower triangular, its eigenvalues are the eigenvalues of A_{11}, A_{22}, A_{33}, and A_{44}, respectively. Using this Kalman decomposition, we obtain $\mathcal{O}_0(s) = C_2 (sI - A_{22})^{-1} B_2$. Consequently, the eigenvalues of A_{11}, A_{33}, and A_{44} are the ones that are canceled in the derivation of the transfer function of (20), (22). Using Design Criterion 5, Remark 7, and Remark 2, it follows that A_{11}, A_{33}, and A_{44} are Hurwitz.

Consider now the complementary sensitivity function

$$\mathcal{T}(s) = \frac{y_{\mathcal{P}_0}(s)}{r(s)} = \frac{\mathcal{P}_0(s)\mathcal{C}_0(s)}{1 + \mathcal{P}_0(s)\mathcal{C}_0(s)}. \tag{23}$$

The following state-space model, derived from (20), (22), describes the dynamics between $r(t)$ and $y_{\mathcal{P}_0}(t)$:

$$\begin{aligned} \dot{\bar{x}}(t) &= \bar{A}_{\mathcal{T}} \bar{x}(t) + \bar{B}_{\mathcal{O}_0} r(t) \\ y_{\mathcal{P}_0}(t) &= \bar{C}_{\mathcal{O}_0} \bar{x}(t) \end{aligned} \tag{24}$$

with

$$\begin{aligned} \bar{A}_{\mathcal{T}} &= \bar{A}_{\mathcal{O}_0} - \bar{B}_{\mathcal{O}_0} \bar{C}_{\mathcal{O}_0} \\ &= \begin{bmatrix} A_{11} & 0 & 0 & 0 \\ A_{21} - B_2 C_1 & A_{22} - B_2 C_2 & 0 & 0 \\ A_{31} & 0 & A_{33} & 0 \\ A_{41} - B_4 C_1 & A_{42} - B_4 C_2 & A_{43} & A_{44} \end{bmatrix}. \end{aligned} \tag{25}$$

From (i) in Proposition 8 we know that $\mathcal{T}(s)$ in (23) has all poles in the open LHP. Since it holds that $\mathcal{T}(s) = C_2(sI - [A_{22} - B_2C_2])B_2$ and $([A_{22} - B_2C_2], B_2, C_2)$ is minimal, this implies that $[A_{22} - B_2C_2]$ is a Hurwitz matrix. From the lower triangular structure of $\bar{A}_{\mathcal{T}}$ and the fact that A_{11}, A_{33}, and A_{44} are Hurwitz, we conclude that $\bar{A}_{\mathcal{T}}$ is Hurwitz. Using the similarity transformation $x = T\bar{x}$, we obtain

$$\begin{aligned} A_{\mathcal{T}} = T \bar{A}_{\mathcal{T}} T^{-1} &= T(\bar{A}_{\mathcal{O}_0} - \bar{B}_{\mathcal{O}_0} \bar{C}_{\mathcal{O}_0}) T^{-1} \\ &\overset{(21)}{=} A_{\mathcal{O}_0} - B_{\mathcal{O}_0} C_{\mathcal{O}_0}. \end{aligned}$$

Using (22), it can be verified that $A_{\mathcal{O}_0} - B_{\mathcal{O}_0} C_{\mathcal{O}_0} = A$, with A given in (12). As such, we conclude that A is Hurwitz, which completes the proof. □

Appendix B
Proof of Theorem 11

Proof: Consider a similarity transformation $\xi = T^{-1}x$, using a nonsingular matrix T, that transforms (A, B, C) of system (11) into the Kalman decomposition

$$\dot{\xi}_1 = \tilde{A}_{11}\xi_1 + \tilde{F}_1 \upsilon \tag{26a}$$

$$\dot{\xi}_2 = \tilde{A}_{21}\xi_1 + \tilde{A}_{22}\xi_2 + \tilde{B}_2 w + \tilde{F}_2 \upsilon \tag{26b}$$

$$\dot{\xi}_3 = \tilde{A}_{31}\xi_1 + \tilde{A}_{33}\xi_3 + \tilde{F}_3 \upsilon \tag{26c}$$

$$\dot{\xi}_4 = \tilde{A}_{41}\xi_1 + \tilde{A}_{42}\xi_2 + \tilde{A}_{43}\xi_3 + \tilde{A}_{44}\xi_4 + \tilde{B}_4 w + \tilde{F}_4 \upsilon \tag{26d}$$

with output

$$\zeta = \tilde{C}_1\xi_1 + \tilde{C}_2\xi_2 + D_\upsilon \upsilon \tag{26e}$$

and input

$$w = -\alpha(\theta)\zeta. \tag{26f}$$

Note that by hypothesis (I), the matrices $\tilde{A}_{11}$, $\tilde{A}_{22}$, $\tilde{A}_{33}$, and $\tilde{A}_{44}$ (suppose they are present) are Hurwitz (due to the lower triangular structure).

In the remainder of the proof, we show that for each subsystem (26), there exists an ISS Lyapunov function (ISSLF) $V_i(\xi_i) = \xi_i^\top P_i \xi_i$, $P_i = P_i^\top \succ 0$, $i = 1, 2, 3, 4$. Clearly, V_i satisfies

$$\lambda_{\min}(P_i)|\xi_i|^2 \leq V_i(\xi_i) \leq \lambda_{\max}(P_i)|\xi_i|^2 \tag{27}$$

in which $\lambda_{\min}(P_i)$, $\lambda_{\max}(P_i)$ denotes the minimum eigenvalue and the maximum eigenvalue of P_i, $i = 1, 2, 3, 4$, respectively. Combining the existence of such ISSLF for each subsystem using a cascade-like argument, see [25], implies that the complete system (26) is ISS with respect to υ. In fact, we will construct an ISSLF for the overall system (11).

Subsystem 1: Since $\tilde{A}_{11}$ is Hurwitz, there exist a quadratic positive definite ISSLF satisfying (27) for $i = 1$, and

$$\dot{V}_1 \leq -c_1|\xi_1|^2 + \gamma_1|\upsilon|^2 \tag{28}$$

with $c_1, \gamma_1 > 0$.

Subsystem 2: Note that $\mathcal{G}(s) = \tilde{C}_2(sI - \tilde{A}_{22})^{-1}\tilde{B}_2$ as subsystem 2 corresponds to the observable and controllable part of the system (11). Hence, using the Kalman–Yakubovich–Popov lemma, see [19, Lemma 6.3], minimality of $(\tilde{A}_{22}, \tilde{B}_2, \tilde{C}_2)$ (as it corresponds to the controllable and observable part of the Kalman decomposition), and under hypothesis (II) of the

theorem, there exist matrices L, $P_2 = P_2^\top \succ 0$, and a positive constant ε_2 such that

$$\tilde{A}_{22}^\top P_2 + P_2\tilde{A}_{22} = -L^\top L - \varepsilon_2 P_2$$
$$P_2\tilde{B}_2 = \tilde{C}_2^\top - \sqrt{\frac{2}{\rho}}L^\top. \tag{29}$$

Let us take $V_2(\xi_2) = \xi_2^\top P_2\xi_2$ as a candidate ISSLF, satisfying (27) for $i = 2$, and for which the time derivative yields

$$\begin{aligned}
\dot{V}_2 &= \xi_2^\top(\tilde{A}_{22}^\top P_2 + P_2\tilde{A}_{22})\xi_2 + 2\xi_2^\top P_2\tilde{B}_2 w \\
&\quad + 2\xi_2^\top P_2\tilde{A}_{21}\xi_1 + 2\xi_2^\top P_2\tilde{F}_2\upsilon \\
&\overset{(29)}{=} -\varepsilon_2 V_2 - \xi_2^\top L^\top L\xi_2 + 2\xi_2^\top\left(\tilde{C}_2^\top - \sqrt{\frac{2}{\rho}}L^\top\right)w \\
&\quad + 2\xi_2^\top P_2\tilde{A}_{21}\xi_1 + 2\xi_2^\top P_2\tilde{F}_2\upsilon \\
&\overset{(26e)}{=} -\varepsilon_2 V_2 - \xi_2^\top L^\top L\xi_2 + 2\zeta w - 2\xi_1^\top\tilde{C}_1^\top w - 2\upsilon^\top D_\upsilon^\top w \\
&\quad + 2\sqrt{\frac{2}{\rho}}\xi_2^\top L^\top w + 2\xi_2^\top P_2\tilde{A}_{21}\xi_1 + 2\xi_2^\top P_2\tilde{F}_2\upsilon.
\end{aligned}$$

Using $w = -\alpha(\theta)\zeta$, with $\alpha(\theta) \in [0, 1]$ for all $\theta(t) \in \Theta$, this yields

$$\begin{aligned}
\dot{V}_2 &\le -\varepsilon_2 V_2 - \xi_2^\top L^\top L\xi_2 - 2w^2 - 2\xi_1^\top\tilde{C}_1^\top w - 2\upsilon^\top D_\upsilon^\top w \\
&\quad + 2\sqrt{\frac{2}{\rho}}\xi_2^\top L^\top w + 2\xi_2^\top P_2\tilde{A}_{21}\xi_1 + 2\xi_2^\top P_2\tilde{F}_2\upsilon \\
&= -\varepsilon_2 V_2 - \left[L\xi_2 + \sqrt{\frac{2}{\rho}}w\right]^\top\left[L\xi_2 + \sqrt{\frac{2}{\rho}}w\right] \\
&\quad - \underbrace{\left(2 - \frac{2}{\rho}\right)}_{=:\phi} w^2 - 2\xi_1^\top\tilde{C}_1^\top w - 2\upsilon^\top D_\upsilon^\top w \\
&\quad + 2\xi_2^\top P_2\tilde{A}_{21}\xi_1 + 2\xi_2^\top P_2\tilde{F}_2\upsilon \\
&\le -\varepsilon_2 V_2 - \phi w^2 - 2\xi_1^\top\tilde{C}_1^\top w - 2\upsilon^\top D_\upsilon^\top w \\
&\quad + 2\xi_2^\top P_2\tilde{A}_{21}\xi_1 + 2\xi_2^\top P_2\tilde{F}_2\upsilon \\
&\overset{(27)}{\le} -\kappa_2|\xi_2|^2 - \phi w^2 - 2\xi_1^\top\tilde{C}_1^\top w - 2\upsilon^\top D_\upsilon^\top w \\
&\quad + 2\xi_2^\top P_2\tilde{A}_{21}\xi_1 + 2\xi_2^\top P_2\tilde{F}_2\upsilon
\end{aligned}$$

for $\kappa_2 := \varepsilon_2\lambda_{\min}(P_2) > 0$, and where we used the fact that $-2w^2 = -\frac{2}{\rho}w^2 - (2-(2/\rho))w^2$ for $\rho \neq 0$. In fact, according to the hypothesis of the theorem, $\rho > 1$, which yields $\phi = (2 - (2/\rho)) > 0$. Using the relation $2ab \le \delta a^2 + (1/\delta)b^2$, which holds for all $a, b \in \mathbb{R}$ and all $\delta > 0$, we obtain

$$\dot{V}_2 \le -c_2|\xi_2|^2 - c_w|w|^2 + \hat{c}_2|\xi_1|^2 + \gamma_2|\upsilon|^2 \tag{30}$$
$$\le -c_2|\xi_2|^2 + \hat{c}_2|\xi_1|^2 + \gamma_2|\upsilon|^2 \tag{31}$$

for some $c_2, c_w, \hat{c}_2, \gamma_2 > 0$. Hence, V_2 is indeed an ISSLF for subsystem 2 with respect to υ and ξ_1. Consequently, one can show based on (28) and (31) that $V_{12} := \mu_1 V_1 + V_2$, for $\mu_1 > 0$ sufficiently large, is an ISSLF for the cascaded system comprising of subsystems 1 and 2, the dynamics of which are given by

$$\begin{bmatrix}\dot{\xi}_1 \\ \dot{\xi}_2\end{bmatrix} = \begin{bmatrix}\tilde{A}_{11}\xi_1 + \tilde{F}_1\upsilon \\ \tilde{A}_{21}\xi_1 + \tilde{A}_{22}\xi_2 + \tilde{B}_2 w + \tilde{F}_2\upsilon\end{bmatrix}$$

and (26e), (26f). Indeed, for sufficiently large μ_1, we would obtain that

$$\dot{V}_{12} \le -c_{12}|\xi_1|^2 - c_{12}|\xi_2|^2 + \gamma_{12}|\upsilon|^2 \tag{32}$$

for some $c_{12}, \gamma_{12} > 0$.

Subsystem 3: Since $\tilde{A}_{33}$ is Hurwitz, there exists a quadratic positive definite ISSLF satisfying (27) for $i = 3$, and

$$\dot{V}_3 \le -c_3|\xi_3|^2 + \hat{c}_3|\xi_1|^2 + \gamma_3|\upsilon|^2 \tag{33}$$

with $c_3, \hat{c}_3, \gamma_3 > 0$. Based on (32) and (33), we can easily see that $V_{123} := \mu_2 V_{12} + V_3$, for sufficiently large $\mu_2 > 0$, satisfies

$$\dot{V}_{123} \le -c_{123}|\xi_1|^2 - c_{123}|\xi_2|^2 - c_{123}|\xi_3|^2 + \gamma_{123}|\upsilon|^2 \tag{34}$$

for some $c_{123}, \gamma_{123} > 0$, and hence is an ISSLF for the cascaded system consisting of subsystems 1–3, the dynamics of which is given by

$$\begin{bmatrix}\dot{\xi}_1 \\ \dot{\xi}_2 \\ \dot{\xi}_3\end{bmatrix} = \begin{bmatrix}\tilde{A}_{11}\xi_1 + \tilde{F}_1\upsilon \\ \tilde{A}_{21}\xi_1 + \tilde{A}_{22}\xi_2 + \tilde{B}_2 w + \tilde{F}_2\upsilon \\ \tilde{A}_{31}\xi_1 + \tilde{A}_{33}\xi_3 + \tilde{F}_3\upsilon\end{bmatrix}$$

and (26e), (26f).

Subsystem 4: Since $\tilde{A}_{44}$ is Hurwitz, there exist a quadratic positive definite ISSLF satisfying (27) for $i = 4$, and [using again $2ab \le \delta a^2 + (1/\delta)b^2$, for $a, b \in \mathbb{R}$ and $\delta > 0$]

$$\begin{aligned}
\dot{V}_4 &\le -c_4|\xi_4|^2 + \hat{c}_4|\xi_1|^2 + \bar{c}_4|\xi_2|^2 + \tilde{c}_4|\xi_3|^2 \\
&\quad + \check{a}_4|w|^2 + \gamma_4|\upsilon|^2
\end{aligned} \tag{35}$$

with $c_4, \hat{c}_4, \bar{c}_4, \tilde{c}_4, \check{a}_4, \gamma_4 > 0$. Using (26e) and (26f), we obtain that $|w|^2 \le q_1|\xi_1|^2 + q_2|\xi_2|^2 + q_\upsilon|\upsilon|^2$, with $q_1, q_2, q_\upsilon > 0$, where we used that $\alpha(\theta) \in [0, 1]$ for all $\theta(t) \in \Theta$. As such, for sufficiently large $c_4, \hat{c}_4, \bar{c}_4, \tilde{c}_4, \gamma_4 > 0$, we have that

$$\dot{V}_4 \le -c_4|\xi_4|^2 + \hat{c}_4|\xi_1|^2 + \bar{c}_4|\xi_2|^2 + \tilde{c}_4|\xi_3|^2 + \gamma_4|\upsilon|^2. \tag{36}$$

Based on (34) and (36), we can establish that $V_{1234} := \mu_3 V_{123} + V_4$, for sufficiently large $\mu_3 > 0$, satisfies

$$\begin{aligned}
\dot{V}_{1234} &\le -c_{1234}|\xi_1|^2 - c_{1234}|\xi_2|^2 - c_{1234}|\xi_3|^2 \\
&\quad - c_{1234}|\xi_4|^2 + \gamma_{1234}|\upsilon|^2
\end{aligned} \tag{37}$$

for some $c_{1234}, \gamma_{1234} > 0$, and hence is an ISSLF for the cascaded systems consisting of subsystems 1–4 the dynamics of which are given by (26). According to [20], this implies (26) and, hence, the original system (11) is ISS with respect to υ, and guarantees the existence of a $\mathcal{KL}$-function β and $\mathcal{K}$-function γ such that the conditions of Definition 10 are satisfied. Moreover, the specific form of (37) implies that the origin of (11) is GES for $\upsilon = 0$, which completes the proof. □

REFERENCES

[1] H. Butler, "Position control in lithographic equipment [applications of control]," *Control Syst. Mag.*, vol. 31, no. 5, pp. 28–47, Oct. 2011.

[2] D. Liberzon, *Switching in Systems and Control*. Boston, MA, USA: Birkhauser, 2003.

[3] M. Steinbuch, J. van Helvoort, W. Aangenent, B. de Jager, and R. van de Molengraft, "Data-based control of motion systems," in *Proc. IEEE Conf. Control Appl.*, Aug. 2005, pp. 529–534.

[4] M. Steinbuch and M. L. Norg, "Advanced motion control: An industrial perspective," *Eur. J. Control*, vol. 4, no. 4, pp. 278–293, 1998.
[5] G. F. Franklin, J. D. Powel, and A. Emami-Naeini, *Feedback Control of Dynamic Systems*. 5th ed. Englewood Cliffs, NJ, USA: Prentice-Hall, 2006.
[6] M. J. van de Wal, G. van Baars, F. Sperling, and O. H. Bosgra, "Multivariable $\mathcal{H}_\infty/\mu$ feedback control design for high-precision wafer stage motion," *Control Eng. Pract.*, vol. 10, no. 7, pp. 739–755, Jul. 2002.
[7] W. J. Rugh and J. S. Shamma, "Research on gain scheduling," *Automatica*, vol. 36, no. 10, pp. 1401–1425, Oct. 2000.
[8] D. J. Leith and W. E. Leithead, "Survey of gain-scheduling analysis and design," *Int. J. Control*, vol. 73, no. 11, pp. 1001–1025, 2000.
[9] M. G. Wassink, M. van de Wal, C. Scherer, and O. Bosgra, "LPV control for a wafer stage: Beyond the theoretical solution," *Control Eng. Pract.*, vol. 13, pp. 231–245, Feb. 2005.
[10] J. S. Shamma and M. Athans, "Guaranteed properties of gain scheduled control for linear parameter-varying plants," *Automatica*, vol. 27, no. 3, pp. 559–564, May 1991.
[11] C. W. Scherer, "LPV control and full block multipliers," *Automatica*, vol. 37, no. 3, pp. 361–375, 2001.
[12] B. Hencey and A. G. Alleyne, "A robust controller interpolation design technique," *IEEE Trans. Control Syst. Technol.*, vol. 18, no. 1, pp. 1–10, Jan. 2010.
[13] W. P. M. H. Heemels, B. De Schutter, J. Lunze, and M. Lazar, "Stability analysis and controller synthesis for hybrid dynamical systems," *Philos. Trans. Roy. Soc. London A, Math. Phys. Sci.*, vol. 368, no. 1930, pp. 4937–4960, 2010.
[14] G. S. Deaecto, J. C. Geromel, and J. Daafouz, "Dynamic output feedback H_∞ control of switched linear systems," *Automatica*, vol. 47, no. 8, pp. 1713–1720, Aug. 2011.
[15] D. J. Leith and W. E. Leithead, "Appropriate realization of gain-scheduled controllers with application to wind turbine regulation," *Int. J. Control*, vol. 65, no. 2, pp. 223–248, 1996.
[16] S. J. L. M. van Loon, R. van der Weijst, M. F. Heertjes, and W. P. M. H. Heemels, "Scheduled controller design for systems with two switching sensor configurations: A frequency-domain approach," in *Proc. IFAC Conf. Anal. Design Hybrid Syst. (ADHS)*, Atlanta, GA, USA, 2015, pp. 99–105.
[17] V. M. Martinez and T. F. Edgar, "Control of lithography in semiconductor manufacturing," *IEEE Control Syst. Mag.*, vol. 26, no. 6, pp. 46–55, Dec. 2006.
[18] L. Zaccarian and A. R. Teel, "A common framework for anti-windup, bumpless transfer and reliable designs," *Automatica*, vol. 38, no. 10, pp. 1735–1744, 2002.
[19] H. K. Khalil, *Nonlinear Systems*. Englewood Cliffs, NJ, USA: Prentice-Hall, 2000.
[20] E. D. Sontag and Y. Wang, "On characterizations of the input-to-state stability property," *Syst. Control Lett.*, vol. 24, no. 5, pp. 351–359, 1995.
[21] M. Arcak and A. R. Teel, "Input-to-state stability for a class of Lurie systems," *Automatica*, vol. 38, no. 11, pp. 1945–1949, Nov. 2002.
[22] M. F. Heertjes and H. Nijmeijer, "Self-tuning of a switching controller for scanning motion systems," *Mechatronics*, vol. 22, no. 3, pp. 310–319, Apr. 2012.
[23] M. Vidyasagar, *Nonlinear Sytems Analysis*. Philadelphia, PA, USA: SIAM, 2002.
[24] V. A. Yakubovich, G. A. Leonov, and A. K. Gelig, *Stability of Stationary Sets in Control Systems With Discontinuous Nonlinearities*. Singapore: World Scientific, 2004.
[25] E. D. Sontag, "Input to state stability: Basic concepts and results," in *Nonlinear and Optimal Control Theory* (Lecture Notes in Mathematics), vol. 1932, Berlin, Germany: Springer, 2008, pp. 163–220.

Robert van der Weijst received the M.Sc. degree in mechanical engineering from the Eindhoven University of Technology, Eindhoven, The Netherlands, in 2014, where he is currently pursuing the Ph.D. degree with the Control Systems Technology Group, Department of Mechanical Engineering.

His current research interests include nonlinear control and extremum seeking optimization for automotive systems.

Bas van Loon received the M.Sc. and the Ph.D. degrees in control systems technology from the Eindhoven University of Technology, Eindhoven, The Netherlands, in 2011 and 2016, respectively.

Since 2016, he has been with DEMCON macawi respiratory systems, Eindhoven, where he has been involved in the development of ventilation and control algorithms for respiratory modules. His current research interests include nonlinear control of linear systems and modeling and control of hybrid systems.

Marcel Heertjes received the M.Sc. and Ph.D. degrees in mechanical engineering from the Eindhoven University of Technology, Eindhoven, The Netherlands, in 1995 and 1999, respectively.

In 2000, he joined the Philips Center for Industrial Technology, Eindhoven. In 2007, he joined ASML, Mechatronics Development, Veldhoven, The Netherlands, and the Control System Technology and the Dynamics and Control groups, Department of Mechanical Engineering, Eindhoven University of Technology, where he holds a position of part-time Associate Professor. His current research interests include the control of industrial motion systems with special focus on nonlinear control, feed forward and learning control, and data-driven optimization and self-tuning.

He was a recipient of the IEEE Control Systems Technology Award 2015 for variable gain control and its applications to wafer scanners and is Associate Editor of the *IFAC Mechatronics*.

Maurice Heemels received the M.Sc. (*summa cum laude*) degree in mathematics and the Ph.D. (*summa cum laude*) degree in control theory from the Eindhoven University of Technology (TU/e), The Netherlands, in 1995 and 1999, respectively.

From 2000 to 2004, he was with the Electrical Engineering Department, TU/e, where he was with the Embedded Systems Institute from 2004 to 2006. In 2004, he was also with the Company Océ, The Netherlands. Since 2006, he has been with the Department of Mechanical Engineering, TU/e, where he is currently a Full Professor. He held visiting professor positions with ETH Zürich, Zürich, Switzerland, in 2001, and with the University of California at Santa Barbara, Santa Barbara, CA, USA, in 2008. His current research interests include hybrid and cyber-physical systems, networked and event-triggered control systems, and constrained systems, including model predictive control.

Dr. Heemels served/s on the Editorial Board of the *Automatica*, the *Nonlinear Analysis: Hybrid Systems*, the *Annual Reviews in Control*, and the IEEE TRANSACTIONS ON AUTOMATIC CONTROL. He was a recipient of the Personal VICI Grant Award by STW (Dutch Technology Foundation).